J|A|C|S ARTICLES

Published on Web 01/02/2009

Pleomorphic Copper Coordination by Alzheimer's Disease Amyloid-β Peptide

Simon C. Drew,[*,†,‡,§,||] Christopher J. Noble,[⊥,#] Colin L. Masters,[§,▽] Graeme R. Hanson,[⊥,#] and Kevin J. Barnham[†,‡,§]

Department of Pathology and Neuroproteomics Platform, National Neuroscience Facility, The Bio21 Molecular Science and Biotechnology Institute, The University of Melbourne, Victoria 3010, Australia, Mental Health Research Institute, The University of Melbourne, Victoria 3010, Australia, School of Physics, Monash University, Victoria 3800, Australia, The University of Queensland, Centre for Magnetic Resonance and Centre for Metals in Biology, Queensland 4072, Australia, and Centre for Neuroscience, The University of Melbourne, Victoria 3010, Australia

Received October 14, 2008; E-mail: sdrew@unimelb.edu.au

Abstract: Numerous conflicting models have been proposed regarding the nature of the Cu^{2+} coordination environment of the amyloid β (Aβ) peptide, the causative agent of Alzheimer's disease. This study used multifrequency CW-EPR spectroscopy to directly resolve the superhyperfine interactions between Cu^{2+} and the ligand nuclei of Aβ, thereby avoiding ambiguities associated with introducing point mutations. Using a library of Aβ16 analogues with site-specific ^{15}N-labeling at Asp1, His6, His13, and His14, numerical simulations of the superhyperfine resonances delineated two independent 3N1O Cu^{2+} coordination modes, {N_a^{D1}, O, N_ε^{H6}, N_ε^{H13}} (component Ia) and {N_a^{D1}, O, N_ε^{H6}, N_ε^{H14}} (component Ib), between pH 6−7. A third coordination mode (component II) was identified at pH 8.0, and simulation of the superhyperfine resonances indicated a 3N1O coordination sphere involving nitrogen ligation by His6, His13, and His14. No differences were observed upon ^{17}O-labeling of the phenolic oxygen of Tyr10, confirming it is not a key oxygen ligand in the physiological pH range. Hyperfine sublevel correlation (HYSCORE) spectroscopy, in conjunction with site-specific ^{15}N-labeling, provided additional support for the common role of His6 in components Ia and Ib, and for the assignment of a {O, N_ε^{H6}, N_ε^{H13}, N_ε^{H14}} coordination sphere to component II. HYSCORE studies of a peptide analogue with selective ^{13}C-labeling of Asp1 revealed ^{13}C cross-peaks characteristic of equatorial coordination by the carboxylate oxygen of Asp1 in component Ia/b coordination. The direct resolution of Cu^{2+} ligand interactions, together with the key finding that component I is composed of two distinct coordination modes, provides valuable insight into a range of conflicting ligand assignments and highlights the complexity of Cu^{2+}/Aβ interactions.

Introduction

Alzheimer's disease (AD) is a neurodegenerative disorder characterized by progressive cognitive and memory impairment.[1] Genetic evidence implicates the amyloid β (Aβ) peptide as the reputed causative agent of the disease. The presence of amyloid plaques, consisting largely of insoluble Aβ aggregates in the brain, is the pathological marker of AD.[1] However, the progression of AD correlates with the concentration of soluble Aβ rather than the concentration of amyloid plaques.[2,3] Metal ions such as copper, iron, and redox silent zinc are found in high concentrations within the plaques.[4,5] Both Cu and Zn coordinated to Aβ have been extracted from post-mortem AD brain.[6] Growing evidence suggests that Cu ions play an important role in the pathogenesis of AD via an oxidative stress pathway.[7]

It is generally accepted that the three His residues of Aβ are involved in high-affinity Cu^{2+} coordination, but the manner in which they coordinate, together with the potential involvement

† Department of Pathology, The University of Melbourne.
‡ Bio21 Molecular Science and Biotechnology Institute, The University of Melbourne.
§ Mental Health Research Institute, The University of Melbourne.
|| Monash University.
⊥ Centre for Magnetic Resonance, The University of Queensland.
Centre for Metals in Biology, The University of Queensland.
▽ Centre for Neuroscience, The University of Melbourne.

(1) Selkoe, D. J. *Physiol. Rev.* **2001**, *81*, 741–766.
(2) McLean, C. A.; Cherny, R. A.; Fraser, F. W.; Fuller, S. J.; Smith, M. J.; Beyreuther, K.; Bush, A. I.; Masters, C. L. *Ann. Neurol.* **1999**, *46*, 860–866.
(3) Lue, L. F.; Kuo, Y. M.; Roher, A. E.; Brachova, L.; Shen, Y.; Sue, L.; Beach, T.; Kurth, J. H.; Rydel, R. E.; Rogers, J. *Am. J. Pathol.* **1999**, *155*, 853–862.
(4) Smith, M. A.; Richey Harris, P. L.; Sayre, L. M.; Beckman, J. S.; Perry, G. *J. Neurosci.* **1997**, *17*, 2653–2657.
(5) Lovell, M. A.; Robertson, J. D.; Teesdale, W. J.; Campbell, J. L.; Markesbery, W. R. *J. Neurol. Sci.* **1998**, *158*, 47–52.
(6) Opazo, C.; Huang, X.; Cherny, R. A.; Moir, R. D.; Roher, A. E.; White, A. R.; Cappai, R.; Masters, C. L.; Tanzi, R. E.; Inestrosa, N. C.; Bush, A. I. *J. Biol. Chem.* **2002**, *277*, 40302–40308.
(7) Bush, A. I. *Alzheimer Dis. Assoc. Disord.* **2003**, *17*, 147–150.
(8) Kowalik-Jankowska, T.; Ruta, M.; Wiśniewska, K.; Łankiewicz, L. *J. Inorg. Biochem.* **2003**, *96*, 270–282.
(9) Syme, C. D.; Nadal, R. C.; Rigby, S. E.; Viles, J. H. *J. Biol. Chem.* **2004**, *279*, 18169–18177.

of the N-terminal amino nitrogen (N_a)[8−11] and the side-chain carboxylate oxygen (O_c) of Asp1, Glu3, Asp7, and Glu11,[8,11−13] remains contentious. A pH-dependent equilibrium between two distinct species has been identified in continuous-wave electron paramagnetic resonance (CW-EPR) spectra of Aβ/Cu^{2+} complexes, commonly designated as "component I" and "component II", with the former being most prevalent at physiological pH. Potentiometric and spectroscopic data of Kowalik-Jankowska and co-workers suggested a {N_a^{D1}, O_c, N_{Im}^{H13}, N_{Im}^{H14}} coordination sphere for component I and {N_a^{D1}, N^-, CO, N_{Im}^{H6}} coordination for component II.[8] Viles and co-workers assigned a {N_a^{D1}, N_{Im}^{H6}, N_{Im}^{H13}, N_{Im}^{H14}} coordination sphere to the dominant Cu^{2+}/Aβ complex at physiological pH, with the involvement of deprotonated amide nitrogens at higher pH.[9,14] Faller and co-workers[11] proposed a model in which component I was characterized by {O_c^{D1}, N_{Im}^{H6}, N_{Im}^{H13}, N_{Im}^{H14}} coordination, with a {N_a^{D1}, N_{Im}^{H6}, N_{Im}^{H13}, N_{Im}^{H14}} coordination sphere for component II. Early Raman spectroscopy[15] suggested the phenolic oxygen of Tyr10 as a possible ligand, an assignment for which a range of evidence has subsequently deemed unlikely.[8−12,16] Theoretical calculations using a model His13-His14 fragment have predicted distorted square-planar {H_2O, N_ε^{H13}, CO^{H13}, N_ε^{H14}} and {H_2O, N_ε^{H13}, N_{am}^{H14}, N_ε^{H14}} coordination modes as the most likely species at pH 7, where it was assumed that the water ligand could be replaced by either N_ε^{H6} or N_a^{D1}.[17] Szalai and co-workers proposed a {N_a^{D1}, O, N_{Im}^{H6}, N_{Im}^{H13}} coordination for component I.[10] Their observation that mutation or removal of Asp1 led to an apparent increase in the ratio of component II/component I signals in the CW-EPR spectra led to a proposal in which the carboxyl oxygen of Asp1 participates not in direct Cu^{2+} coordination but rather in hydrogen-bonding interactions with either an axial water or a deprotonated backbone amide.[13] Studies of Aβ4−16 revealed dramatic differences in the CW-EPR spectra in which the dominant species corresponded to neither component I nor component II.[10] This sequence eliminated the carboxylate side chains of both Asp1 and Glu3 as potential ligands; however, it also engendered the truncated peptide with the high-affinity ATCUN motif (NH_2-Xaa-Yaa-His sequence). This enabled the possibility of particularly stable coordination of terminal amino, two deprotonated amide and imidazole nitrogen donor atoms in fused (5,5,6)-membered chelate rings,[18] a mode normally inaccessible by the native peptide in the physiological pH range.

EXAFS studies have proposed a distorted six-coordinated (3N3O) geometry at pH 7.4, including the three histidines, glutamic, or/and aspartic acid side chains and axial water.[12] ^{1}H NMR studies of ^{15}N-labeled Aβ40 in the presence of 0.05 equiv of Cu^{2+} showed upfield shift movements for the side-chain aromatic signals of the three histidines but no evidence of ^{1}H NMR chemical shift movements of Asp1 or the Tyr10 side chain at pH 7.3.[16] Similarly, recent electron spin echo envelope modulation (ESEEM) studies of Cu^{2+}/Aβ16(^{15}N-His6), Cu^{2+}/Aβ16(^{15}N-His13), and Cu^{2+}/Aβ16(^{15}N-His14) at pH 7.4 also directly implicated all three His residues.[19] However, all of these results were obtained at or near physiological pH, where the coexistence of components I and II might be expected to produce an average picture of Cu^{2+} coordination.[8,9,13]

The many contrasting findings outlined above show that the nature of the metal−ligand interactions in Cu^{2+}/Aβ complexes remains unclear and requires a means for experimentally determining the contribution of each residue to the pH-dependent Cu^{2+} coordination. CW-EPR is capable of making this determination, provided resonances arising from the superhyperfine (shf) resonances can be resolved. In the $g_\perp$ region of the CW-EPR spectrum, the peak separations of the shf resonances are governed by the orientation-dependent hyperfine interactions of the unpaired electron with the Cu^{2+} nucleus and each of the ligand nuclei, the magnitudes of which depend on the strength of the nuclear magnetic moment, the s electron density at the nucleus, and the orientation and distance of the nucleus from the Cu^{2+} ion. The shf resonances are frequently hidden beneath the inhomogeneous line width or obscured because of excessively large modulation amplitudes. Using copper enriched in either ^{65}Cu or ^{63}Cu rather than natural abundance (69% ^{63}Cu, 31% ^{65}Cu) to reduce the inhomogeneous line width and employing modulation amplitudes that are much less than the separation of the shf resonances can help to improve spectral resolution.

When ^{14}N shf resonances can be directly resolved in the CW-EPR spectrum, the reliance on more indirect assignments based upon the empirical Blumberg−Peisach relations can be reduced.[20] However, it can still be difficult to discriminate between $2 \times {}^{14}$N and $3 \times {}^{14}$N coordination or between $3 \times {}^{14}$N and $4 \times {}^{14}$N coordination using numerical simulations because (i) the center of gravity of the shf resonances may not appreciably shift, (ii) the additional satellite resonances associated with more nitrogen-rich coordination modes are frequently buried in the noisy wings of the spectrum, and (iii) the variation in the intensity profile of 3N versus 4N coordination may only be subtle.[21] This potential ambiguity can be overcome by selective ^{15}N-labeling of specific ligand nuclei, which imposes additional constraints on the number and strength of shf couplings. Site-specific isotopic labeling involves a change of both the nuclear spin and magnetic moment of a nucleus, which visibly alters the appearance of the shf resonances whenever the labeled atom is a Cu^{2+} ligand and provides a means to determine the number and type of Cu^{2+} ligands directly from the CW-EPR spectrum. Moreover, for noncoordinating ligand nuclei >4 Å from the Cu^{2+}, the positions of cross-peaks in two-dimensional hyperfine sublevel correlation (HYSCORE) spectra will also be affected as a result of isotopic labeling and hence the outer coordination sphere of Cu^{2+} can also be probed.

We synthesized a library of Aβ analogues with isotopic labeling of specific residues − Aβ16(^{15}N^{13}C-Asp1), Aβ16(^{17}O-Tyr10), Aβ16(^{15}N-His6), Aβ16(^{15}N-His13), Aβ16(^{15}N-His14), and triple-labeled Aβ16(^{15}N-His6,13,14) − and analyzed their shf interactions in the presence of substoichiometric $^{65}Cu^{2+}$ using

(10) Karr, J. W.; Akintoye, H.; Kaupp, L. J.; Szalai, V. A. *Biochemistry* **2005**, *44*, 5478–5787.
(11) Guilloreau, L.; Damian, L.; Coppel, Y.; Mazarguil, H.; Winterhalter, M.; Faller, P. *J. Biol. Inorg. Chem.* **2006**, *11*, 1024–1038.
(12) Streltsov, V. A.; Titmuss, S. J.; Epa, V. C.; Barnham, K. J.; Masters, C. L.; Varghese, J. N. *Biophys. J.* **2008**, *95*, 3447–3456.
(13) Karr, J. W.; Szalai, V. A. *J. Am. Chem. Soc.* **2007**, *129*, 3796–3797.
(14) It is unclear whether the amino terminus was explicitly implicated in the higher pH coordination associated with component II.
(15) Miura, T.; Suzuki, K.; Kohata, N.; Takeuchi, H. *Biochemistry* **2000**, *39*, 7024–7031.
(16) Hou, L.; Zagorski, M. G. *J. Am. Chem. Soc.* **2006**, *128*, 9260–9261.
(17) Raffa, D. F.; Gómez-Balderas, R.; Brunelle, P.; Rickard, G. A.; Raux, A. *J. Biol. Inorg. Chem.* **2005**, *10*, 887–902.
(18) Sóvágó, I.; Ősz, K. *Dalton Trans.* **2006**, 3841–3854.
(19) Shin, B.; Saxena, S. *Biochemistry* **2008**, *47*, 9117–9123.
(20) Peisach, J.; Blumberg, W. E. *Arch. Biochem. Biophys.* **1974**, *165*, 691–698.
(21) Drew, S. C.; Djoko, K. Y.; Zhang, L.; Koay, M.; Boas, J. F.; Pilbrow, J. R.; Xiao, Z.; Barnham, K. J.; Wedd, A. G. *J. Biol. Inorg. Chem.* **2008**, *13*, 899–907.

Table 1. Aβ16 Peptide Sequences Used in This Study; Labeled Residues Appear in Boldface

Aβ16	DAEFRHDSGYEVHHQK-OH
Aβ16(^{15}N^{13}C-Asp1)[a]	**D**AEFRHDSGYEVHHQK-OH
Aβ16(^{17}O-Tyr10)[b]	DAEFRHDSG**Y**EVHHQK-OH
Aβ16(^{15}N-His6)[c]	DAEFR**H**DSGYEVHHQK-OH
Aβ16(^{15}N-His13)[c]	DAEFRHDSGYEV**H**HQK-OH
Aβ16(^{15}N-His14)[c]	DAEFRHDSGYEVH**H**QK-OH
Aβ16(^{15}N-His6,13,14)[c]	DAEFR**H**DSGYEV**HH**QK-OH

[a] ^{15}N^{13}C-Asp = ^{15}**N**H$_2$^{13}**C**H(^{13}**C**H$_2$^{13}**C**OOH)^{13}**C**OOH. [b] ^{17}O-Tyr = NH$_2$CH(CH$_2$C$_6$H$_4$**^{17}O**H)COOH. [c] ^{15}N-His = ^{15}**N**H$_2$CH(CH$_2$C$_3$^{15}**N**$_2$H$_3$)-COOH.

a combination of CW and pulsed EPR. Working with Aβ16 as a model for the longer 39−42 residue peptide minimizes issues surrounding peptide aggregation that arise when the hydrophobic C-terminus of Aβ is present, which may cause a loss of spectral resolution. We show that the main species identified in the CW-EPR spectra of Cu^{2+}/Aβ complexes (component I) is composed of two interconverting 3N1O coordination modes anchored upon the amino terminus and the imidazole side chain of His6, with the third nitrogen ligand swapping between the imidazole side chains of His13 and His14. We further show that component II is characterized by a coordination sphere involving all three His residues, while the amino terminus no longer coordinates. The phenolic oxygen of Tyr10 does not provide an oxygen ligand in any of the coordination modes that dominate components I and II signals. HYSCORE spectroscopy in conjunction with selective ^{13}C-labeling of Asp1 reveals that the side chain carboxylate of Asp1 is not an oxygen ligand in component II coordination, but provides evidence for its participation in a stable six-membered chelate ring in component I.

Experimental Section

Peptide Synthesis. Table 1 lists the peptides synthesized for this study. Fmoc-L-Asp(O-^{t}Bu)-OH (uniform ^{13}C, >98%; ^{15}N, >98%), Fmoc-L-His(Trt)-OH (uniform ^{15}N, 98%), and L-tyrosine (phenol-^{17}O, 35%) were purchased from Cambridge Isotope Laboratories, Inc. Peptide synthesis was carried out in the Peptide Technology Facility of the Bio21 Molecular Science and Biotechnology Institute, The University of Melbourne. Unlabeled Aβ16 (DAEFRHDSGYEVHHQK-OH) was synthesized by solid-phase peptide synthesis on Fmoc-L-Lys(Boc)-PEG-PS resin (Applied Biosystems) using a CEM Liberty microwave peptide synthesizer. Aβ16(^{15}N^{13}C-Asp1) was similarly synthesized using the CEM Liberty microwave peptide synthesizer, with the N-terminal Fmoc-L-^{15}N-Asp(O-^{t}Bu)-OH being manually coupled at the end of the synthesis. During the synthesis of Aβ16(^{15}N-His6), Aβ16(^{15}N-His13), Aβ16(^{15}N-His14), and Aβ16(^{15}N-His6,13,14), Fmoc-L-^{15}N-His(Trt)-OH was manually coupled and the remainder of the peptide was assembled on the CEM Liberty peptide synthesizer. The ^{17}O-tyrosine was protected as the Fmoc-L-^{17}O-Tyr-OH derivative. Residues 11−16 of Aβ16 (^{17}O-Tyr10) were synthesized on the CEM Liberty peptide synthesizer, and the final 10 amino acids were manually coupled. The peptides were purified by RP-HPLC, and the product was verified by Q-TOF mass spectrometry. Final peptide purity was determined to be 98−99% using the final RP-HPLC trace.

Sample Preparation. The lyophilized Aβ16 peptides were suspended in phosphate-buffered saline pH 7.4 (Amresco) at a concentration of ∼0.7−1.0 mM, as determined using an extinction coefficient at 280 nm of 1280 M^{-1} cm^{-1}. Glycerol was added at 10% v/v to ensure good glass formation upon subsequent freezing. ^{65}CuO (>99% ^{65}Cu, Cambridge Isotope Laboratories) was dissolved by stirring in concentrated HCl and diluted in milliQ water to prepare a 10 mM stock of ^{65}CuCl$_2$. For X-band CW-EPR, 0.3 molar equiv of ^{65}CuCl$_2$ was added to the peptide solution. For S-band CW-EPR and pulsed EPR studies, 0.9 molar equiv of ^{65}CuCl$_2$ was added. Isotopically enriched ^{65}Cu was used to avoid inhomogeneous broadening of the resonance lines due to the different magnetic moments of the natural isotopes (69% ^{63}Cu, $g_n = 1.485$; 31% ^{65}Cu, $g_n = 1.588$). The pH was measured using a microprobe (Hanna Instruments) and adjusted to 6.3, 6.9, or 8.0 (±0.1) using concentrated NaOH or HCl. Samples were transferred to quartz EPR tubes (Wilmad, SQ-707) and snap frozen in liquid nitrogen.

CW-EPR Spectroscopy. X-band CW-EPR was performed using a Bruker ESP380E spectrometer fitted with a rectangular TE_{102} microwave cavity and a quartz coldfinger insert. Microwave frequencies were measured with an EIP Microwave 548A frequency counter, and g factors were calibrated against the F^+ line in CaO ($g = 2.0001 \pm 0.0002$).[22] Experimental conditions were: microwave power, 10 mW; microwave frequency, 9.42 GHz; modulation amplitude, 4 G; modulation frequency, 100 kHz; temperature, 77 K; sweep time, 168 s; time constant, 164 ms; eight averages. Background correction was performed by subtraction of the sample-free spectrum. S-band CW-EPR was carried out using a Bruker Elexsys E500 spectrometer fitted with a split ring S-band resonator (Bruker) and a variable-temperature nitrogen flow system. Frequencies were measured with an EIP 548B microwave frequency counter. Experimental conditions were: microwave power, 10 mW; microwave frequency, 4.04 GHz; modulation amplitude, 2 G; modulation frequency, 100 kHz; temperature, 130 K; sweep time, 42 s; time constant, 10.24 ms; 100 averages. Second derivative spectra were obtained by differentiating the first harmonic spectrum, followed by Fourier filtering using a Hamming window to remove high frequency noise, ensuring the spectrum was not distorted.

CW-EPR simulations were performed using version 1.1.4 of the XSophe-Sophe-XeprView computer simulation software[23] on an i686 PC running Mandriva 2007 using the following spin Hamiltonian:

$$H = \beta \mathbf{B}\cdot\mathbf{g}\cdot\mathbf{S} + \mathbf{S}\cdot\mathbf{A}\cdot\mathbf{I} - g_n\beta_n\mathbf{B}\cdot\mathbf{I} + \sum_k (\mathbf{S}\cdot{}^k\mathbf{A}\cdot{}^k\mathbf{I} - {}^k g_n\beta_n\mathbf{B}\cdot{}^k\mathbf{I}) \quad (1)$$

where **S** and **I** are the electron and nuclear vector spin operators, **g** and **A** are the 3 × 3 electron Zeeman and ^{65}Cu hyperfine coupling matrixes, β is the Bohr magneton, β_n is the nuclear magneton, and **B** is the applied magnetic field. The summation incorporates the superhyperfine and nuclear Zeeman interactions with ligand nuclei k of spin ^kI and nuclear g factor ^kg_n. Axial symmetry was assumed ($g_x = g_y = g_\perp$, $g_z = g_\parallel$; $A_x = A_y = A_\perp$, $A_z = A_\parallel$). For the directly coordinated nitrogen nuclei, the principal $^kA_\parallel$ and $^kA_\perp$ directions of the shf interaction lie approximately parallel and perpendicular to the metal−ligand bond directions (cf. $g_\parallel$ and $A_\parallel$, which are directed perpendicular to the metal−ligand bonding plane). However, the ligand shf couplings are dominated by the Fermi contact interaction, which renders the ^{k}**A** approximately isotropic. Hence, to reduce computational effort, the in-plane ligand shf coupling (resolvable in the $g_\perp$ region of the spectrum) was assumed isotropic and equal to a_k. Matrix diagonalization was used to determine the main transitions in conjunction with high-order perturbation theory to further solve for the electron−nuclear shf transitions. Component I simulations utilized the spectra at pH 6.3 to avoid spectral contamination from component II signals near physiological pH. Distributions of the principal g and A parameters of ^{65}Cu were included using the g and A strain line width model.[24,25] More accurate principal g values were determined from X-band spectra.

(22) Wertz, J. E.; Orton, J. W.; Auzins, P. *Discuss. Faraday Soc.* **1961**, *31*, 140–150.
(23) Hanson, G. R.; Gates, K. E.; Noble, C. J.; Griffin, M.; Mitchell, A.; Benson, S. *J. Inorg. Biochem.* **2004**, *98*, 903–916.
(24) Hyde, J. S.; Froncisz, W. *Annu. Rev. Biophys. Bioeng.* **1982**, *11*, 391–417.
(25) Pilbrow, J. R. *Transition Ion Electron Paramagnetic Resonance*; Clarendon Press: Oxford, 1990.

Table 2. Spin Hamiltonian Parameters of Cu^{2+}/Aβ16 Complexes, Determined from Simulations of the CW-EPR Spectra in Figures 3 and 4; Selected Spin Hamiltonian Parameters of Component I and II Signals from Other Work Are Included for Comparison, Together with the Proposed Mode of Coordination, Where Applicable

component I	$g_{\|}$	$g_{\perp}$	$A_{\|}(^{63}Cu)^a$	$A_{\perp}(^{63}Cu)^a$	$a(^{14}N_a^{D1})^b$	$a(^{14}N_{\varepsilon}^{H6})^b$	$a(^{14}N_{\varepsilon}^{H13/14})^b$	ref
			component I					
Aβ16 {N_a^{D1}, O, N_{ε}^{H6}, N_{ε}^{H13}} component Ia	2.272 ± 0.005	2.056 ± 0.005	171 ± 3	14.5 ± 0.5	11.3 ± 0.5	13.0 ± 0.5	14.0 ± 0.5	c
{N_a^{D1}, O, N_{ε}^{H6}, N_{ε}^{H14}} component Ib								
Aβ16 {N_a^{D1}, O_c, N_{Im}^{H13}, N_{Im}^{H14}}	2.262	n.d.[d]	185	n.d.	n.d.	n.d.	n.d.	8
Aβ16 {N_a^{D1}, N_{Im}^{H6}, N_{Im}^{H13}, N_{Im}^{H14}}	2.26[g]	2.06[g]	187[g]	n.d.	n.d.	n.d.	n.d.	9
Aβ16 {N_a^{D1}, O, N_{Im}^{H6}, N_{Im}^{H13}}	2.269 ± 0.001		180 ± 2	n.d.[f]	n.d.	n.d.	n.d.	13
Aβ40 fibrils	2.268 ± 0.001	2.061 ± 0.002	178 ± 1	n.d.	n.d.	n.d.	n.d.	47
			component II					
Aβ16 {O, N_{ε}^{H6}, N_{ε}^{H13}, N_{ε}^{H14}}	2.227 ± 0.003	2.043 ± 0.003	157 ± 3	21.0 ± 1.0	15.0 ± 1.0	12.5 ± 1.0	12.5 ± 1.0	c
Aβ16, Aβ28 {N_a^{D1}, N^-, CO, N_{Im}^{H6}}	2.229	n.d.	162	n.d.	n.d.	n.d.	n.d.	8
Aβ16, Aβ28	2.226	n.d.	162 ± 1	n.d.	n.d.	n.d.	n.d.	13
Aβ16, Aβ28	2.22[g]	2.06[g]	176[g]	n.d.	n.d.	n.d.	n.d.	9

[a] All hyperfine parameters are expressed in units of 10^{-4} cm^{-1} (1×10^{-4} cm^{-1} = 2.9979 MHz). Where hyperfine data was given in gauss (G) in the original reference, it was converted into wavenumbers using the expression $A_{\|}$ (10^{-4} cm^{-1}) = $10^4(g_{\|}\beta_e/hc) \times A_{\|}$ (G), where h is Plank's constant, c = 2.9979×10^{10} cm s^{-1} and $\beta_e = 9.274 \times 10^{-28}$ J G^{-1}. [b] Tabulated superhyperfine couplings are given as their ^{14}N equivalent using the conversion factor $|g_n(^{15}N)/g_n(^{14}N)| = 1.40$. [c] This work. To aid comparison with other work in which natural abundance copper (69% ^{63}Cu, 31% ^{65}Cu) was used, hyperfine couplings were converted from ^{65}Cu to those expected for ^{63}Cu using the scaling factor $|g_n(^{65}Cu)/g_n(^{63}Cu)| = 1.07$. Uncertainties in hyperfine couplings represent the estimated range. [d] n.d. = not determined. [e] $g_x = 2.048 \pm 0.003$, $g_y = 2.065 \pm 0.003$. [f] Although values of A_x(Cu) and A_y(Cu) were given, these were not explicitly resolved in the experimental spectra and the line widths used in numerical simulations were larger than A_x(Cu) and A_y(Cu). [g] Parameters were first-order estimates obtained by direct measurement of spectral splittings in gauss rather than numerical simulation; component II splitting of 170 G at X-band appears to be in large error compared with other literature values. The conversion from $A_{\|}$[G] into $A_{\|}$[milliKaiser] (0.1 mK = 1×10^{-4} cm^{-1}) in ref 9 also used $g_e = 2.0023$ instead of $g_{\|}$.

The spectral parameters were optimized using a simplex algorithm within the XSophe-Sophe-XeprView computer simulation software,[23] whereby the principal A parameters of the metal ion, the ligand shf couplings, and the g and A strain parameters were varied iteratively to minimize the root mean square error between the experimental and simulated spectra.

We note at this stage that use of ^{65}Cu-enriched copper leads to different values of $A_{\|}$ compared with other CW-EPR studies of Cu^{2+}/Aβ complexes in which natural abundance copper is used (Table 2). To enable closer comparison of our results with earlier studies, we scaled our ^{65}Cu hyperfine couplings to the equivalent values for ^{63}Cu, since this is the most abundant natural isotope (69% ^{63}Cu, 31% ^{65}Cu). Our tabulated $A_{\|}(^{63}Cu)$ couplings therefore appeared smaller compared with hyperfine couplings determined using natural abundance copper, since the latter yields values intermediate between $A_{\|}(^{63}Cu)$ and $A_{\|}(^{65}Cu)$, which differ because of their distinct nuclear magnetic moments ($g_n(^{65}Cu)/g_n(^{63}Cu)$ = 1.07).

HYSCORE Spectroscopy. X-band ESEEM experiments were performed using a Bruker ESP380E spectrometer fitted with a Bruker ER 4118 dielectric resonator, an Oxford Instruments CF935 cryostat and an ITC4 temperature controller, and a 1kW TWT amplifier. The two-dimensional HYSCORE experiments were carried out at 15 K using a $\pi/2$-τ-$\pi/2$-t_1-π-t_2-$\pi/2$-τ-echo sequence, with pulse lengths $t_{\pi/2}$ = 16 ns and t_{π} = 24 ns, and a four-step phase cycle was used to eliminate unwanted echoes. Orientation-selective spectra were obtained at magnetic fields corresponding to $g_{\|}$ and/or $g_{\perp}$ (Figure S6 in the Supporting Information). The time intervals t_1 and t_2 were varied from 48 to 8240 ns in steps of 64 ns (Nyquist frequency of 7.81 MHz); a value of τ = 144 ns was used to help keep the spectrum free of blind spots[26] below 7 MHz and to suppress proton modulation and subsequent frequency foldback of the ^1H Larmor frequency. All data were acquired using the same microwave attenuation and resonator coupling position to enable the comparison of different spectra. The real part of the time-domain quadrature signal was selected, then background-corrected using a second-order polynomial fit, zero-filled, and apodized with a Hamming window function. Following 2D-FFT, the absolute value was computed and the two-dimensional spectra were symmetrized about the diagonal by setting $S(\nu_j,\nu_i) = S(\nu_i,\nu_j) = \min[S(\nu_i,\nu_j), S(\nu_j,\nu_i)]$ to minimize artifacts. Spectra were normalized by the maximum intensity observed in the frequency domain spectrum. Only the (+,+) quadrant of the frequency domain was plotted, since no prominent peaks were observed in the (−,+) quadrant. HYSCORE simulations were carried out using Floquet theory with the MolecularSophe computer simulation software suite[27] on an i686 PC running Mandriva 2007.

The ESEEMs of spectra of $S = {}^1/_2$, $I = 1$ systems such as those involving $^{14}N_{\varepsilon}$ coordination from His side chains are well-characterized.[28,29] At X-band frequencies, approximate cancelation of the nuclear Zeeman and electron−nuclear hyperfine interactions between Cu^{2+} and the distal imidazole $^{14}N_{\delta}$ takes place, such that the energy level splitting within the ^{14}N superhyperfine spin manifold is determined primarily by the nuclear quadrupole interaction $\mathbf{I}\cdot\mathbf{Q}\cdot\mathbf{I}$. This matching condition ($2\nu_I \approx a_{iso}$) leads to deep modulations of the electron spin echo at or near the nuclear quadrupole frequencies. For orientationally disordered systems, these appear as cross-peaks at (ν_{α}^{dq},ν_{β}^{dq}) and (ν_{β}^{dq},ν_{α}^{dq}) in the HYSCORE spectrum, correlating the double-quantum ($|\Delta m_I| = 2$) transitions within the α and β electron spin manifolds. For an axial hyperfine interaction, the hyperfine matrix in its principal axis system can be expressed as A = ($a_{iso} - T$, $a_{iso} - T$, $a_{iso} + 2T$), wherein the point-dipole approximation the anisotropic coupling is given by $T = (\mu_0/4\pi)g\beta g_n\beta_n/r^3$, μ_0 is the permeability of vacuum, and r is the

(26) Schweiger, A.; Jeschke, G. *Principles of Pulse Electron Paramagnetic Resonance*; Oxford University Press: Oxford, 2001.

(27) Hanson, G. R.; Noble, C. J.; Benson, S. *High Resolution EPR*; Hanson, G., Berliner, L., Eds.; Biological Magnetic Resonance 28; Springer Publishing: New York, 2009; Chapter 4, pp 105−174.

(28) Deligiannakis, Y.; Louloudi, M.; Hadjiliadis, N. *Coord. Chem. Rev.* **2000**, *204*, 1–112.

(29) McCracken, J.; Pember, S.; Benkovic, S. J.; Villafranca, J. J.; Miller, R. J.; Peisach, J. *J. Am. Chem. Soc.* **1988**, *110*, 1069–1074.

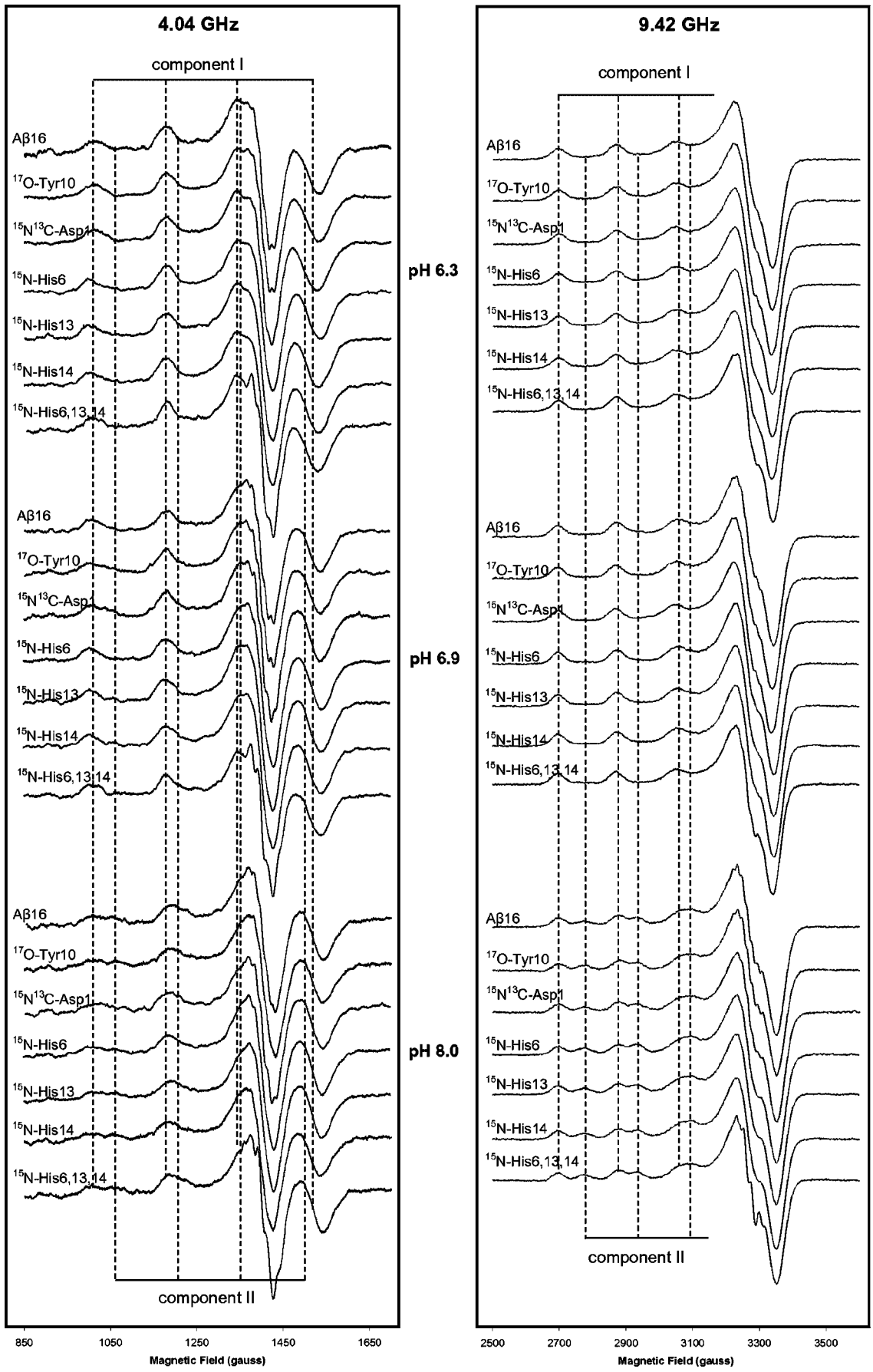

Figure 1. S-band (4.04 GHz) and X-band (9.42 GHz) CW-EPR spectra of Cu^{2+}/Aβ16 and labeled Cu^{2+}/Aβ16 complexes obtained with substoichiometric ^{65}Cu at pH 6.3, 6.9, and 8.0. Dashed vertical lines identify the position of the resolved features corresponding to components I and II.

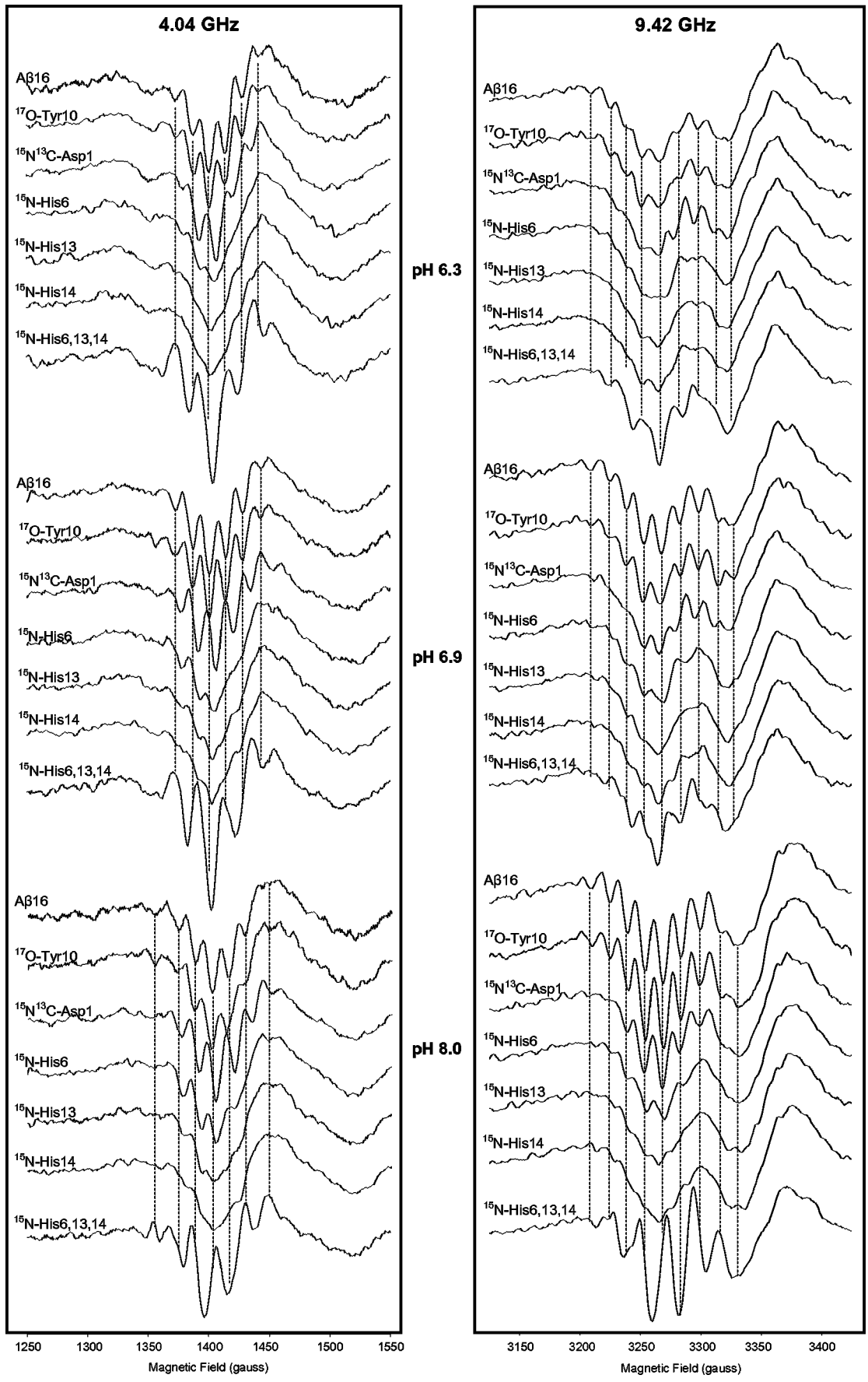

Figure 2. Second derivative multifrequency CW-EPR spectra of Cu^{2+}/Aβ16 and labeled Cu^{2+}/Aβ16 complexes at pH 6.3, 6.9, and 8.0, expanded around the superhyperfine resonances in the $g_\perp$ region. For comparative purposes, dashed vertical lines identify the position of some of the resolved features of the native Cu^{2+}/Aβ16 complex.

internuclear distance. When the anisotropic hyperfine coupling T is small compared with a_{iso}, the double quantum frequencies are given by the second-order resonance condition:[26,28,29]

$$\nu_{\alpha(\beta)}^{dq} = 2[(\nu_I \mp |a_{iso}|/2)^2 + K^2(3+\eta^2)]^{1/2} \quad (2)$$

Here ν_I is the ^{14}N Larmor frequency, a_{iso} is the isotropic coupling, $K = e^2qQ/4h$, Q is the nuclear quadrupole moment, q is the electric field gradient at the nucleus, h is Planck's constant, and the quadrupole asymmetry parameter η lies in the range [0,1]. In the instance where ^{15}N is substituted for ^{14}N, or when ^{13}C is substituted for ^{12}C, the ESEEM is described by an $S = {}^1/_2$, $I = {}^1/_2$ system and the correlation peak positions are given by the first-order resonance condition:

$$\nu_{\alpha(\beta)} = \nu_I \mp |a_{iso}|/2 \quad (3)$$

When the anisotropic hyperfine interaction is non-negligible, the correlation peaks of an orientationally averaged 2D spectrum become ridges, as described by Dikanov and Bowman.[30] Similar to the $I = 1$ case, strong spectral features are expected under the matching condition $2\nu_I \approx a_{iso}$ (T small).

Results

Multifrequency CW-EPR Spectroscopy. The CW-EPR spectra of the Cu^{2+}/Aβ complexes obtained at both S-band (4.04 GHz) and X-band (9.42 GHz) are displayed in Figure 1, which shows that both frequencies were capable of resolving the shf resonances within the $g_\perp$ region (ca. 1400 and 3300 G at S- and X-band, respectively). To resolve the shf resonances at X-band, a relatively low Cu^{2+} loading (0.3 equiv) was required, whereas at S-band 0.9 equiv of Cu^{2+} could be used since g and A strain broadening effects are reduced at lower microwave frequency.[24] This reduction in line broadening sometimes also enables resolution of shf resonances directly from within the M_I (^{65}Cu) $= -{}^1/_2$ line of the S-band spectra; however, this was not possible in the present case. Nevertheless, the smaller electron Zeeman interaction at S-band led to increased state mixing and enhanced second-order effects on resonant field positions, which produced shf spectra at $g_\perp$ that were generally better resolved, especially at lower pH. The shf resonances were more easily discerned in the second derivative presentation of the spectra, which is shown expanded about the $g_\perp$ region in Figure 2.

The pattern of shf resonances observed in the spectra of all ^{15}N-labeled analogues deviated significantly from the native Cu^{2+}/Aβ16 spectrum (Figure 2), indicating that N_a^{D1}, N_ε^{H6}, N_ε^{H13}, and N_ε^{H14} are each involved in pH-dependent Cu^{2+} coordination.[31] The spectrum of the Cu^{2+}/Aβ16(^{17}O-Tyr10) complex, on the other hand, was not significantly different from the native peptide at pH 6.3, 6.9, and 8.0 (Figure 2). The magnitude of superhyperfine coupling for equatorially coordinated $^{17}O(I = {}^5/_2)$ to type II Cu^{2+} is expected to be $\sim 11 \times 10^{-4}$ cm^{-1}, and therefore clear differences in the $g_\perp$ region and a broadening of the low-field ^{65}Cu hyperfine resonances should have been apparent,[32] compared with that of the native Cu^{2+}/Aβ spectrum, if Tyr10 is a ligand. This provided direct evidence

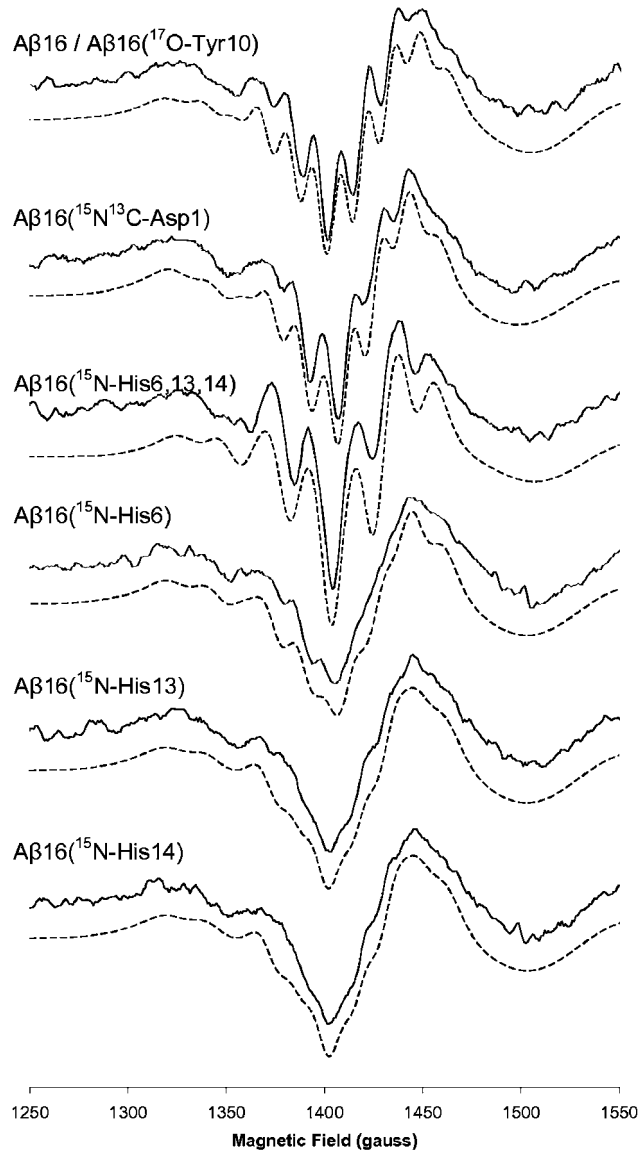

Figure 3. Comparison of experimental (full lines) and simulated (dashed lines) second derivative S-band (4.04 GHz) CW-EPR spectra of $^{65}Cu^{2+}$/Aβ16 and various isotopically labeled analogues at pH 6.3 (expanded about the $g_\perp$ region). The spectra were modeled as a weighted summation of two coordination modes as described in the text (Figure 5). The simulation parameters appear in Table 2.

that the side chain of Tyr10 is not an oxygen ligand in the physiological pH range and confirmed a range of data[8−12] disputing the early putative assignment.[15,33] At pH < 7, numerical simulations of the CW-EPR spectrum of native Cu^{2+}/Aβ16 could be fitted to a 3 × ^{14}N coordination sphere, with shf couplings of $a_1(^{14}N) = (11.3 \pm 0.5) \times 10^{-4}$ cm^{-1}, $a_2(^{14}N) = (13.0 \pm 0.5) \times 10^{-4}$ cm^{-1}, and $a_3(^{14}N) = (14.0 \pm 0.5) \times 10^{-4}$ cm^{-1} (Figure 3). The spectrum of Cu^{2+}/Aβ16($^{15}N^{13}C$-Asp1) could be simulated using the same parameters, but with a_1 scaled by a factor of $g_n(^{15}N)/g_n(^{14}N) = 1.40$ (2 × ^{14}N/1 × ^{15}N coordination), which identified the a_1 shf coupling with the terminal amino nitrogen, N_a.[34] Moreover, the spectrum of the

(30) Dikanov, S. A.; Bowman, M. K. *J. Magn. Reson.* **1995**, *A116*, 125–128.
(31) Although coordination via the pyrrole nitrogen (N_δ) of histidine has been proposed, experimental evidence shows the imidazole nitrogen (N_ε) usually functions as the metal ligand. (See Sundberg, R. J.; Martin, R. B. Chem. Rev. 1974, *74*, 471−516.) Cu^{2+}-induced deprotonation of the amide nitrogen (N_{am}) of histidine is also insignificant at pH 6.3.
(32) Brändén, R.; Deinum, J. *FEBS Lett.* **1977**, 144–146.
(33) Curtain, C. C.; Ali, F.; Volitakis, I.; Cherny, R. A.; Norton, R. S.; Beyreuther, K.; Barrow, C. J.; Masters, C. L.; Bush, A. I.; Barnham, K. J. *J. Biol. Chem.* **2001**, *276*, 20466–20473.
(34) The shf couplings of the noncoordinated ^{13}C atoms of Asp1 are too small to be resolved using CW-EPR spectroscopy.

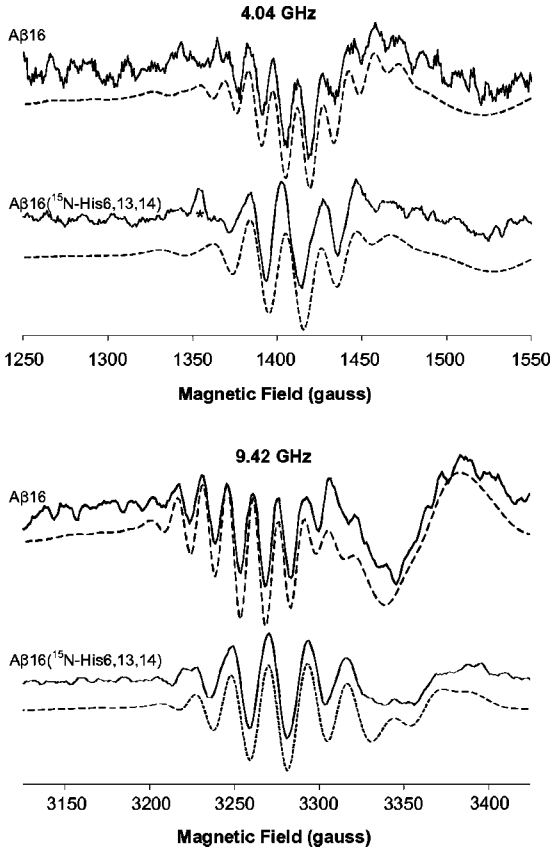

Figure 4. Comparison of experimental (full lines) and simulated (dashed lines) second derivative multifrequency CW-EPR spectra of component II signals of Cu^{2+}/Aβ16 and Cu^{2+}/Aβ16(^{15}N-His6,13,14) complexes, isolated by weighted subtraction of the pH 6.9 spectra from the pH 8.0 spectra in Figure 2. The spectra of Cu^{2+}/Aβ16 were simulated assuming electron−nuclear coupling to the three inequivalent ^{14}N ligand nuclei (Table 2). In the Cu^{2+}/Aβ16(^{15}N-His6,13,14) simulations, the three ^{14}N ligand nuclei were replaced by their ^{15}N equivalents (shf couplings scaled by 1.40). Feature marked with an asterisk is assigned to a spectral artifact.

Cu^{2+}/Aβ16(^{15}N-His6,13,14) complex, in which N_δ, N_ε, and the backbone amide (N_{am}) of all three His residues were ^{15}N-labeled, could be simulated using the same model when a_2 and a_3 were scaled by 1.40 ($1 \times {}^{14}N/2 \times {}^{15}N$ coordination), implicating two magnetically distinct histidine N_ε atoms as ligands (Figure 3).[31] The magnitudes of the shf couplings were consistent with literature values for isotropic hyperfine couplings of N_a and N_ε ligands.[35] Taken together, this established that a {N_a^{D1}, O, $2N_\varepsilon$} coordination mode could be assigned to component I, immediately ruling out models involving simultaneous coordination of all three His residues such as {N_a^{D1}, N_{Im}^{H6}, N_{Im}^{H13}, N_{Im}^{H14}} coordination[9] and {O_c^{D1}, N_{Im}^{H6}, N_{Im}^{H13}, N_{Im}^{H14}} coordination.[11]

In apparent contradiction to a {N_a^{D1}, O, $2N_\varepsilon$} assignment for component I, the shf resonances in the CW-EPR spectra of Aβ16(^{15}N-His6), Aβ16(^{15}N-His13), and Aβ16(^{15}N-His14) peptide analogues also deviated substantially from the unlabeled peptide (Figures 2 and 3), indicating that each of the three His residues coordinate Cu^{2+} at least some of the time. Therefore, additional coordination mode(s) must contribute to the component I signal. Component II coordination is only a minor component at pH 6.9 and insignificant at pH 6.3 (Figure 1). A 2N2O coordination mode with $g_{||} = 2.286$, $A_{||}(^{63}Cu) = 157 \times 10^{-4}$ cm^{-1} was identified by potentiometric measurements at pH < 6;[8] however, there is no evidence for the presence of such a distinctly different mode in the CW-EPR spectra at pH 6.3 (Figure 1). Our observations could be reconciled by assuming the presence of more than one {N_a^{D1}, O, $2N_\varepsilon$} Cu^{2+} coordination mode, such that component I was a weighted summation of overlapping EPR spectra, each with a {N_a^{D1}, O, $2N_\varepsilon$} coordination sphere characterized by similar $g_{||}$ and $A_{||}$ parameters but involving N_ε ligands from different His residues. The ability to simulate the shf spectra of Cu^{2+}/Aβ16, Cu^{2+}/Aβ16(^{15}N^{13}C-Asp1), and Cu^{2+}/Aβ16(^{15}N-His6,13,14) with a single set of shf parameters indicated that the magnitude of the shf couplings of the N_a and N_ε ligands must not vary greatly between each mode.

On the basis of the similarity of the shf spectra of Cu^{2+}/Aβ16(^{15}N-His13) and Cu^{2+}/Aβ16(^{15}N-His14) (Figure 3), we deduced that two {N_a^{D1}, O, $2N_\varepsilon$} coordination modes were present in component I, where the amino terminus and His6 were common ligands but the second N_ε ligand was supplied by His13 or His14, namely {N_a^{D1}, O, N_ε^{H6}, N_ε^{H13}} and {N_a^{D1}, O, N_ε^{H6}, N_ε^{H14}}. In confirmation of this assignment, we were able to simulate Cu^{2+}/Aβ16(^{15}N-His6) using the same model as above, with the a_2 coupling scaled by 1.40 (Figure 3, Table 2), thereby establishing N_ε^{H6} as a common ligand and suggesting that the shf couplings with N_ε^{H13} and N_ε^{H14} in each mode must be approximately the same and equal to a_3. As shown later, HYSCORE spectroscopy also provided evidence for the anchoring role of N_ε^{H6} in both coordination modes. Since His13 and His14 are not ligands common to both modes, the spectra of Cu^{2+}/Aβ16(^{15}N-His13) and Cu^{2+}/Aβ16(^{15}N-His14) needed to be simulated as a summation of two distinctly different spectra. In the case of Cu^{2+}/Aβ16(^{15}N-His13), the first spectrum consisted of a $3 \times {}^{14}N$ coordination sphere characterized by shf couplings a_1, a_2, a_3 as above (corresponding to the {$^{14}N_a^{D1}$, O, $^{14}N_\varepsilon^{H6}$, $^{14}N_\varepsilon^{H14}$} contribution), while the second spectrum was characterized by the same couplings except that a_3 was scaled by 1.40 (corresponding to the {$^{14}N_a^{D1}$, O, $^{14}N_\varepsilon^{H6}$, $^{15}N_\varepsilon^{H13}$} contribution). As shown in Figure S1 in the Supporting Information, a summation of these two spectra in equal proportion was an excellent reproduction of the experimental spectrum, as also indicated in Figure 3. The procedure for simulating Cu^{2+}/Aβ16(^{15}N-His14) was analogous (Figure S2 in the Supporting Information) and, under the assumptions made, led to an identical shf spectrum (Figure 3). The excellent fits to the entire library of labeled peptides (Figure 3) by modeling component I as an equilibrium between {N_a^{D1}, O, N_ε^{H6}, N_ε^{H13}} and {N_a^{D1}, O, N_ε^{H6}, N_ε^{H14}} coordination modes in approximately equal proportion suggest that between pH 6−7 Aβ anchors Cu^{2+} at the amino terminus and the side chain of His6, while His13 and His14 are in rapid exchange.[36] We designated these two modes component Ia and component Ib, respectively.

At pH 8.0, component II was present in equilibrium with components Ia and Ib in the CW-EPR spectra (Figure 1). The principal $g_{||}$ and $A_{||}$ (^{65}Cu) parameters of component II were consistent with literature values determined by other studies (Table 2). The shf resonances corresponding to component II were particularly well-resolved at both S-band and X-band (Figures 1 and 2) and were isolated following a weighted subtraction of the component Ia/b spectrum (Figures 4 and S3 in the Supporting Information). Numerical simulations of the

(35) Baute, D.; Arieli, D.; Neese, F.; Zimmermann, H.; Weckhuysen, B. M.; Goldfarb, D. *J. Am. Chem. Soc.* **2004**, *126*, 11733–11745.

(36) It is also possible that the Cu^{2+} ligands in each mode are supplied by different Aβ monomers rather than from a single macrochelate. EPR cannot easily distinguish between these two possibilities.

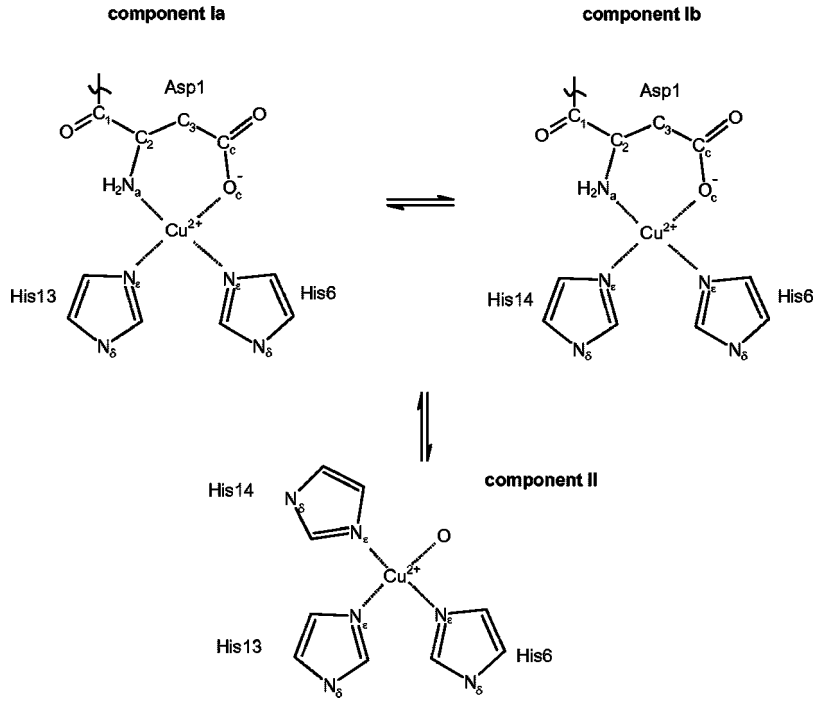

Figure 5. Two-dimensional model of the putative coordination modes responsible for component I and component II signals of Cu^{2+}/Aβ complexes. Superhyperfine interactions with N_a^{D1}, N_ε^{H6}, N_ε^{H13}, and N_ε^{H14} were observed directly using CW-EPR (Figure 3). Interactions with distant N_δ^{H6}, N_δ^{H13}, N_δ^{H14}, and the carbon nuclei of Asp1 were probed using HYSCORE spectroscopy (Figures 6 and 7).

native Cu^{2+}/Aβ16 complex indicated that component II was characterized by a 3 × ^{14}N coordination sphere with $a_1(^{14}N) = (12.5 \pm 1.0) \times 10^{-4}$ cm^{-1}, $a_2(^{14}N) = (12.5 \pm 1.0) \times 10^{-4}$ cm^{-1}, and $a_3(^{14}N) = (15.0 \pm 1.0) \times 10^{-4}$ cm^{-1} (Figure 4, Table 2). A dramatic change in the shf pattern was observed for the component II spectrum of Cu^{2+}/Aβ16(^{15}N-His6,13,14), which was also particularly well-resolved at both S-band and X-band (Figures 1 and 2). The component II spectrum could be simulated by scaling the above a_1, a_2, and a_3 couplings by a factor of $\gamma_n(^{15}N)/\gamma_n(^{14}N) = 1.40$ (Figure 4, Table 2), indicating that the three nitrogen ligands originated from any of the three His residues. Consistent with the above, the component II spectrum of Aβ16(^{15}N^{13}C-Asp1) was very similar to that of the native peptide (Figure S4 in the Supporting Information), confirming the absence of coordination by the amino terminus. Models involving N_a coordination in component II, or the coordination of less than three His nitrogen atoms, such as {N_a^{D1}, N_ε^{H6}, N_ε^{H13}, N_ε^{H14}}[11] and {N_a^{D1}, N^-, CO, N_{Im}^{H6}},[8] are therefore inconsistent with our present findings. Since all three amide and imidazole nitrogen atoms were ^{15}N-labeled, bidentate nitrogen ligation remained a possibility for component II. Although the resolution and signal-to-noise ratio was limited (Figure S5 in the Supporting Information), none of the component II spectra of Cu^{2+}/Aβ16(^{15}N-His6), Cu^{2+}/Aβ16(^{15}N-His13), and Cu^{2+}/Aβ16(^{15}N-His14) showed clear evidence of a 3 × ^{14}N contribution (cf. component Ia and Ib, where Cu^{2+}/Aβ16(^{15}N-His13) and Cu^{2+}/Aβ16(^{15}N-His14) spectra contained ∼50% 3 × ^{14}N contribution). This suggested that the component II signal was due to a single coordination mode only. Moreover, component II spectra of Cu^{2+}/Aβ16(^{15}N-His6), Cu^{2+}/Aβ16(^{15}N-His13), and Cu^{2+}/Aβ16(^{15}N-His14) each differed from the native Cu^{2+}/Aβ16 spectrum (Figure S5 in the Supporting Information), indicating that the three His nitrogen atoms in component II arise from monodentate coordination of His6, His13, and His14. Because of the uniform ^{15}N-labeling of the imidazole and amide nitrogen atoms of histidine, CW-EPR was unable to distinguish between main or side-chain coordination of each histidine. More selective ^{15}N-labeling of individual His nitrogen nuclei would be required to make this distinction using CW-EPR. HYSCORE spectroscopy, on the other hand, is capable of detecting imidazole coordination and, as outlined below, provided evidence for the side-chain coordination of all His residues in component II. It was therefore concluded that a {O, N_ε^{H6}, N_ε^{H13}, N_ε^{H14}} coordination mode is responsible for the component II signal in Cu^{2+}/Aβ16 complexes (Figure 5).

HYSCORE Spectroscopy. To examine the local Cu^{2+} environment beyond the first coordination sphere, HYSCORE spectroscopy was used to detect electron−nuclear couplings between Cu^{2+} and noncoordinated ^{13}C, ^{14}N, and ^{15}N nuclei. The HYSCORE spectra of unlabeled Aβ16 (Figure 6a,b) obtained near the maximum absorption of the echo-detected EPR spectrum (Figure S6 in the Supporting Information) revealed cross-peaks at (1.6, 4.0) and (4.0, 1.6) MHz, characteristic of the double quantum ($|\Delta m_I| = 2$) transitions ν_α^{dq}, ν_β^{dq} of distal imidazole $^{14}N_\delta$ nuclei from coordinating His side chains.[28] At pH 6.3, the HYSCORE spectrum of Aβ16(^{15}N^{13}C-Asp1) (Figure 6c,e) clearly showed an additional pair of cross-peaks centered at the ^{13}C Larmor frequency ($\nu_C = 3.61$ MHz at 3370 G) with a splitting of ∼2.7 MHz and a width of ∼1 MHz. The spectrum measured in the $g_{||}$ region (Figure S7 in the Supporting Information) revealed peaks with a splitting of ∼2.4 MHz and a width of ∼0.6 MHz. From the low orientation selectivity at $g_\perp$, numerical simulations estimated a hyperfine coupling of $a_{iso} = -2.8$ MHz and $T = 0.8$ MHz (Figure 6g). A previous HYSCORE, electron−nuclear double resonance, and density functional theory (DFT) study of Cu^{2+} amino acid complexes determined that the carboxyl $^{13}C_c$ coupling of an equatorially coordinated carboxylate is characterized by a negative a_{iso} with a magnitude of 3−4 MHz, whereas a free or axially coordinated carboxylate group has a small (∼1 MHz) and a positive a_{iso}.[35] Our results were therefore consistent with the assignment of an equatorial carboxylate oxygen ligand from Asp1 in component

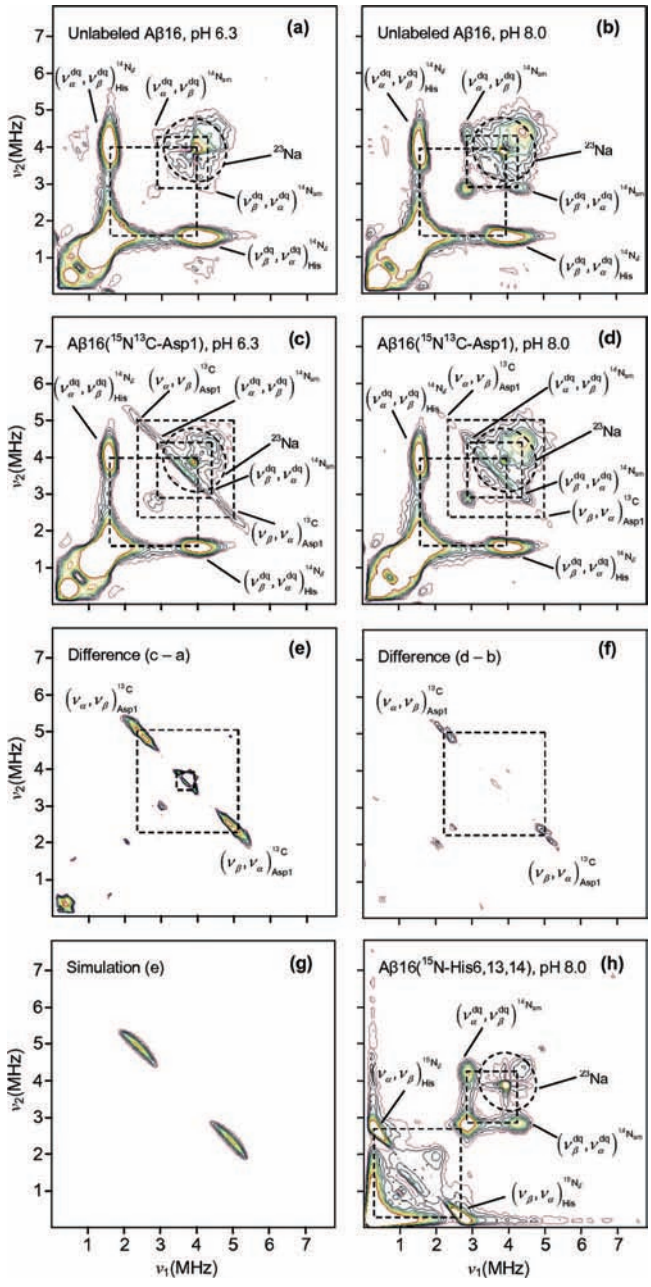

Figure 6. X-band (9.72 GHz) HYSCORE spectra of Cu^{2+}/Aβ16 and Cu^{2+}/Aβ16(^{15}N^{13}C-Asp1), obtained at 3370 G (near $g_\perp$). Cross-peaks at ~(1.6, 4.0) and (4.0, 1.6) MHz (a−d) are diagnostic of $^{14}N_\delta$ His side-chain coordination, while cross-peaks at ~(2.8, 4.2) and (4.2, 2.8) MHz (b, d, h) are consistent with a nearby noncoordinating backbone amide[28,37] with $a_{iso}(^{14}N_{am}) \approx 1$ MHz and $4K \approx 3$ MHz (eq 2). The persistence of the $^{14}N_{am}$ features in the spectra of both Cu^{2+}/Aβ16(^{15}N^{13}C-Asp1) (d) and Cu^{2+}/Aβ16(^{15}N-His6,13,14) (h) indicates that they originate from a residue other than Asp1, His6, His13, and His14. For Cu^{2+}/Aβ16(^{15}N^{13}C-Asp1), additional correlation ridges centered on the ^{13}C Larmor frequency appear (c−f). Simulation of the ^{13}C ridges yielded $a_{iso} = -2.8$ MHz and $T = 0.8$ MHz (g), consistent with equatorial O_c^{D1} coordination.[35] The ^{13}C cross-peaks with splitting <1 MHz (e) are assigned to distant ^{13}C nuclei of Asp1 such as $^{13}C_1$ and $^{13}C_3$ (Figure 5). Contours in spectra e and f are drawn to a scale different from that in a−d. Features at the ^{23}Na Larmor frequency (circled) are from weakly coupled, distant buffer counterions.

I coordination. The CW-EPR simulations established that the amino nitrogen is a ligand at pH 6.3 (Figure 3), which would therefore leave the $^{13}C_2H$ carbon of Asp1 at a similar distance from the Cu^{2+} ion (Figure 5). Heuristically, a greater spin density on $^{13}C_c$ compared with that of $^{13}C_2$ might be expected, since

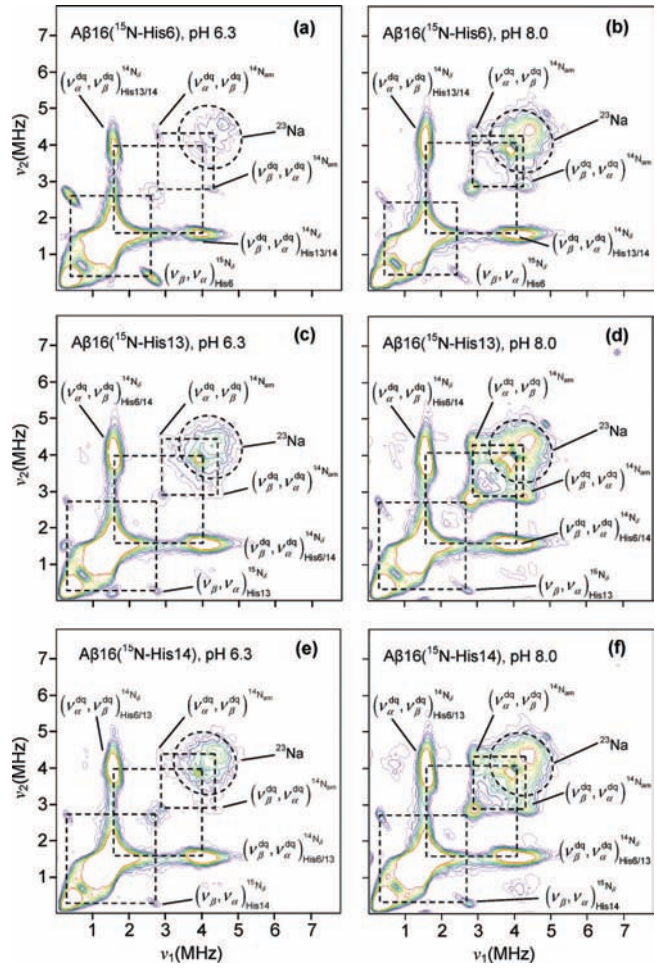

Figure 7. X-band (9.72 GHz) HYSCORE spectra of Cu^{2+}/Aβ16 and labeled Cu^{2+}/Aβ16 analogues, obtained at 3370 G (near $g_\perp$). Selective ^{15}N-labeling of each His residue shifted the $^{14}N_\delta$ features to their ^{15}N equivalents, centered upon the ^{15}N Larmor frequency ($\nu_{15N} = 1.45$ MHz at 3370 G). The typical first-order splitting of $|a_{iso}(^{15}N_\delta)| \approx 2.5$ MHz or $|a_{iso}(^{14}N_\delta)| \approx 1.8$ MHz (eq 3) indicated conditions were close to exact cancelation ($\nu_I = |a_{iso}|/2$) and consistent with imidazole Cu^{2+} coordination.[28] At pH < 7, the relative intensity of the $^{15}N_\delta^{H6}$ cross-peaks (a) was greater than those of the $^{15}N_\delta^{H13}$ (c) and $^{15}N_\delta^{H14}$ cross-peaks (e), providing further evidence for the imidazole side chain of His6 as a common ligand in both components Ia and Ib (Figure 5). The smaller splitting of the $^{15}N_\delta^{H6}$ cross-peaks compared with those of $^{15}N_\delta^{H13}$ and $^{15}N_\delta^{H14}$ suggested a smaller isotropic hyperfine coupling to N_δ^{H6}, consistent with the assignment of a smaller $a_{iso}(N_\varepsilon^{H6})$ from CW-EPR simulations (Figure 3, Table 2). At pH 8.0, the relative intensity of the $^{15}N_\delta^{H6}$, $^{15}N_\delta^{H13}$, and $^{15}N_\delta^{H14}$ cross-peaks is more comparable (b, d, f), supporting the assignment of {O, N_ε^{H6}, N_ε^{H13}, N_ε^{H14}} coordination from CW-EPR simulations of component II (Figure 4).

there are at least two pathways for electron delocalization through the carboxylate oxygen (one σ and one π orbital), whereas the amino nitrogen provides only a single pathway via sp^3 hybridization. However, we cannot definitively rule out the possibility that cross-peaks due to electron−nuclear coupling with $^{13}C_2$ are also present that could potentially mask any $^{13}C_c$ cross-peaks due to equatorial carboxylate coordination. Figure 6e also exhibits another set of cross-peaks centered upon the ^{13}C Larmor frequency, but with a much smaller splitting ($a_{iso} \approx 1$ MHz). These may originate from an axially coordinated or noncoordinated carboxylate oxygen (vide supra) and/or electron−nuclear couplings with the distant $^{13}C_1$ and $^{13}C_3$ carbons of Asp1 (Figure 5). At pH 8.0, the intensity of the ^{13}C cross-peaks was diminished (Figure 6f). Again, it was not possible to distinguish between a loss of N_a^{D1} coordination alone and the loss of

bidentate N_a^{D1},O_c^{D1} coordination. Accurate modeling of the spin density at the C_2 nucleus of Asp1, or a more atom-specific ^{13}C-labeling scheme, is required to definitively determine whether equatorial Asp1 carboxylate coordination occurs in component Ia and Ib coordination modes; however, it can be concluded here that O_c^{D1} is not an oxygen ligand in component II coordination.

At pH 6.3, additional features appeared at ~(2.8, 4.2) and (4.2, 2.8) MHz in the HYSCORE spectra (Figure 6a,c) and particularly intense cross-peaks were also present in the same region at pH 8.0 (Figure 6b,d). These could in principle arise from combination harmonics of ν_α^{dq} and ν_β^{dq};[29] however, they may also arise from nitrogen nuclei where the exact cancelation condition is not fulfilled. In particular, similar features were observed from noncoordinating backbone amide nitrogen atoms in other Cu^{2+} proteins.[28,37,38] To confirm their origin, we examined the Cu^{2+}/Aβ16(^{15}N-His6,13,14) analogue. In this instance, the position of the $^{14}N_\delta$ peaks shifted position to their $^{15}N_\delta$ equivalents centered upon the ^{15}N Larmor frequency (ν_{15N} = 1.45 MHz at 3370 G), whereas the (2.8, 4.2) and (4.2, 2.8) MHz peaks were not shifted (Figure 6h), indicating they did not originate from His residues. We therefore assigned them to a noncoordinating N_{am} from a residue other than His6, His13, or His14 in the second coordination sphere of Aβ, with $a_{iso}(^{14}N_{am}) \approx 1$ MHz and $4K \approx 3$ MHz (eq 2).[28,37]

To further examine the role of each His side chain in Cu^{2+} coordination, HYSCORE spectra of Cu^{2+}/Aβ16(^{15}N-His6), Cu^{2+}/Aβ16(^{15}N-His13), and Cu^{2+}/Aβ16(^{15}N-His14) were also obtained at pH 6.3 and 8.0. Selective ^{15}N-labeling of each His residue shifted the $^{14}N_\delta$ features pertaining to each His residue to their ^{15}N equivalents, centered upon the ^{15}N Larmor frequency (Figure 7). The typical first-order splitting of $|a_{iso}(^{15}N_\delta)| \approx 2.5$ MHz or $|a_{iso}(^{14}N_\delta)| \approx 1.8$ MHz (eq 3) indicated conditions were close to exact cancelation ($\nu_I = |a_{iso}|/2$) and consistent with imidazole Cu^{2+} coordination.[28] Although the modulation depth in the time domain, and hence the cross-peak intensity in the frequency domain, is dependent upon the relative orientation of the principal g and ^kA axes,[26,28] the much greater intensity of the $^{15}N_\delta^{H6}$ cross-peaks compared $^{15}N_\delta^{H13}$ and $^{15}N_\delta^{H14}$ cross-peaks at pH < 7 provided further support for the assignment of the imidazole side chain of His6 as a common ligand in both components Ia and Ib. The smaller splitting of the $^{15}N_\delta^{H6}$ cross-peaks compared with those of $^{15}N_\delta^{H13}$ and $^{15}N_\delta^{H14}$ suggested a smaller isotropic hyperfine coupling to N_δ^{H6}, consistent with the assignment of a smaller $a_{iso}(N_\varepsilon^{H6})$ from CW-EPR simulations (Figure 3, Table 2, eq 3). At pH 8.0, the relative intensity of the $^{15}N_\delta^{H6}$, $^{15}N_\delta^{H13}$, and $^{15}N_\delta^{H14}$ cross-peaks was more comparable, supporting the assignment made from CW-EPR simulations of a {O, N_ε^{H6}, N_ε^{H13}, N_ε^{H14}} coordination sphere in component II.

Discussion

A wealth of experimental evidence indicates that all three His residues of Aβ coordinate Cu^{2+}. However, no study has addressed the potential ambiguity that exists in distinguishing which His residues are involved in each coordination mode, because it is difficult to delineate these contributions from each other. Multifrequency CW-EPR spectroscopy, in conjunction with site-specific isotopic labeling, enabled us to directly analyze the metal−ligand shf resonances to determine the coordination environment of Cu^{2+} rather than rely on the potentially ambiguous Blumberg−Peisach relations between $g_{||}$ and $A_{||}$.[20] In particular, it enabled us to uncover two independent coordination modes within the component I signal that has usually been associated with a single species.

Our finding that component I is composed of {N_a^{D1}, O, N_ε^{H6}, N_ε^{H13}} and {N_a^{D1}, O, N_ε^{H6}, N_ε^{H14}} coordination modes can be reconciled with a number of earlier observations. The potentiometric data of Kowalik−Jankowska and co-workers identified an equilibrium between two species between pH 6−7 for Aβ16, each with similar $g_{||}$ and $A_{||}$ parameters ($g_{||} = 2.262$, $A_{||}(^{63}Cu) = 185 \times 10^{-4}cm^{-1}$) (Table 2). Consistent with our findings, each was assigned a {N_a^{D1}, O_c, $2N_{Im}$} coordination sphere, except that His13 and His14 were suggested to be the likely N_{Im} donors in both.[8] Although Viles and co-workers proposed a dominant {N_a^{D1}, N_{Im}^{H6}, N_{Im}^{H13}, N_{Im}^{H14}} coordination mode at pH 7.4, their combined spectroscopic data suggested that the amino terminus and His13 were crucial for Cu^{2+} binding and that His6 and His14 were also implicated.[9] Szalai and co-workers proposed that the native Cu^{2+} binding site at physiological pH comprised the amino terminus, an unidentified oxygen atom, His6, and His13.[10] Simultaneous coordination of His13 and His14 was ruled out on the basis of the observation that the CW-EPR spectrum of soluble Cu^{2+}/Aβ was nearly identical to that of Cu^{2+} bound to Aβ40 fibrils (Table 2)[10] and a model fibril structure that forced His13 and His14 on opposite sides of parallel β-sheets.[39] Our finding that His13 and His14 are capable of independently coordinating Cu^{2+} in modes with similar principal $g_{||}$ and $A_{||}$ values provides a likely explanation for the similar appearance of the CW-EPR spectra of soluble and fibrillar Cu^{2+}/Aβ at physiological pH.

Models that exclude coordination of the amino terminus in component I, such as {O_c^{D1}, N_ε^{H6}, N_ε^{H13}, N_ε^{H14}},[11] are inconsistent with the present findings, as are models implicating simultaneous coordination of all three histidines, namely {O_c^{D1}, N_ε^{H6}, N_ε^{H13}, N_ε^{H14}},[11] {N_a^{D1}, N_ε^{H6}, N_ε^{H13}, N_ε^{H14}},[9] and {$O_c^{D1/E11}$, N_ε^{H6}, N_ε^{H13}, N_ε^{H14}}.[12] That such assignments were postulated is not surprising, however, since the overlapping component Ia and Ib signals will give the appearance of simultaneous coordination of all three His residues unless spectroscopic methods capable of quantitatively delineating {N_a^{D1}, O, N_ε^{H6}, N_ε^{H13}} and {N_a^{D1}, O, N_ε^{H6}, N_ε^{H14}} are employed.

To isolate component II signals at pH 8.0, a weighted subtraction of the low pH spectra from the respective pH 8.0 spectra was performed. Numerical simulations of the component II shf resonances in the CW-EPR spectrum of the native Cu^{2+}/Aβ16 complex indicated a 3 × ^{14}N coordination sphere, while simulations of the shf resonances of Cu^{2+}/Aβ16(^{15}N-His6,13,14) and Cu^{2+}/Aβ16($^{15}N^{13}$C-Asp1) showed that the nitrogen ligands originated from histidine residues only. The component II shf spectra of Cu^{2+}/Aβ16(^{15}N-His6), Cu^{2+}/Aβ16(^{15}N-His13), and Cu^{2+}/Aβ16(^{15}N-His14), together with HYSCORE spectroscopy, further supported the participation of all three His side chains in a single {O, N_ε^{H6}, N_ε^{H13}, N_ε^{H14}} coordination mode. Models involving N_a as a ligand or the coordination of less than three His nitrogen atoms in component II, such as {N_a^{D1}, N_ε^{H6}, N_ε^{H13},

(37) Jin, H.; Thomann, H.; Coyle, C. L.; Zumft, W. G. *J. Am. Chem. Soc.* **1989**, *111*, 4262–4269.
(38) Burns, C. S.; Aronoff-Spencer, E.; Dunham, C. M.; Lario, P.; Avdievich, N. I.; Antholine, W. E.; Olmstead, M. M.; Vrielink, A.; Gerfen, G. J.; Peisach, J.; Scott, W. G.; Millhauser, G. L. *Biochemistry* **2002**, *41*, 3991–4001.
(39) Morgan, D. M.; Dong, J.; Jacob, J.; Lu, K.; Apkarian, R. P.; Thiyagarajan, P.; Lynn, D. G. *J. Am. Chem. Soc.* **2002**, *124*, 12544–12645.

$N_\varepsilon^{H14}\}$[11] and $\{N_a^{D1}, N^-, CO, N_{Im}^{H6}\}$,[8] are inconsistent with these findings. Theoretical modeling of $Cu^{2+}/A\beta$ interactions based upon a His13-His14 fragment predicted distorted square-planar $\{H_2O, N_\varepsilon^{H13}, CO^{H13}, N_\varepsilon^{H14}\}$ and $\{H_2O, N_\varepsilon^{H13}, N_{am}^{H14}, N_\varepsilon^{H14}\}$ coordination modes as the most likely species at pH 7, where it was assumed that the water ligand could be replaced by either N_ε^{H6} or N_a^{D1}.[17] However, the simultaneous coordination of N_ε^{H13} and N_ε^{H14} is inconsistent with the structure determined for components Ia and Ib, which predominate at pH 7 (Figure 5).

The principal $g_{||}$, $g_\perp$, and $A_{||}$ values determined from the spectral simulations of components Ia and Ib represent average values, and the parameters for both coordination modes fall within the tabulated range of uncertainties (Table 2). The small differences in principal $g_{||}$ values between each mode were evident from the subtle pH-dependent broadening of the low-field ^{65}Cu hyperfine resonance in X-band at pH < 7 (Figure 1). Small differences in $g_\perp$ values for components Ia and Ib resulted in a different center of gravity of their respective shf resonances. At X-band, where the g value resolution was greater, this increased destructive interference and a loss of resolution of the shf resonances (Figure 2). The shf resolution was also generally poorer at X-band because of increased g and A strain broadening effects. The reduced sensitivity of the S-band spectra to small variations in principal g values enabled these confounding effects to be minimized, and hence the multifrequency approach was particularly valuable in this study. There did not appear to be any significant difference in the shf patterns of the ^{15}N-His6, ^{15}N-His13, and ^{15}N-His14 spectra upon moving from pH 6.3 to 6.9 (Figure 2), other than a slight improvement in resolution (common to all spectra). The determination of any subtle changes in the relative population of components Ia and Ib beyond the assumed equal weighting was beyond the limitations of our data.

HYSCORE spectroscopy of the $Cu^{2+}/A\beta$ complexes identified cross-peaks at (2.8, 4.2) and (4.2, 2.8) MHz, consistent with the presence of a nearby noncoordinating nitrogen atom, as observed in other Cu^{2+} proteins.[28,37,38] In the case of the octarepeat Cu^{2+} binding domain (PHGGGWGQ) of the prion protein, similar features were shown to originate from backbone carbonyl coordination that left an amide nitrogen three bonds away from the Cu^{2+} ion.[38] Interestingly, a backbone carbonyl group has been proposed as a ligand for component II coordination (Table 2),[8] although in this instance a $\{N_a^{D1}, N^-, CO, N_{Im}^{H6}\}$ coordination sphere was assumed, which is inconsistent with our finding that three His nitrogen atoms coordinate Cu^{2+} in component II. Quantum chemistry calculations of complexes modeling the His13-His14 portion of $A\beta$ have also proposed oxygen coordination by the backbone carbonyl of His13 as part of a chelate involving N_ε^{H13} and N_ε^{H14}.[17] However, the ^{15}N-labeling data explicitly ruled out the amide nitrogen atoms of histidine residues as a source of the cross-peaks observed in the HYSCORE spectra and therefore do not provide support for such an assignment. Unlike the octarepeat binding domain of the prion protein, $A\beta$ has a number of more favorable oxygen ligands available in the form of the acidic side chains of Glu3, Asp7, and Glu11, for which the molecular models involving only the His13-His14 fragment are unable to account. On the basis of the close similarity of the X-band CW-EPR spectra of copper complexes of $A\beta16$(E3Q), $A\beta16$(D7N), and $A\beta16$(E11Q) with that of the native peptide, it has been suggested that Glu3, Asp7, and Glu11 do not directly coordinate Cu^{2+}.[13] The above conclusions relied upon an absence of any apparent changes in the principal $g_{||}$ and $A_{||}$ parameters of components I and II following the introduction of the point mutations, but the close similarity of the $Cu^{2+}/A\beta16$(H6A), $Cu^{2+}/A\beta16$(H13A), and $Cu^{2+}/A\beta16$(H14A) spectra and the native $Cu^{2+}/A\beta16$ spectrum[9] shows that spectral changes following point mutations are an unreliable indicator of the source of Cu^{2+} ligands. Therefore, the carboxylate side chains of these residues cannot be ruled out in either component Ia, Ib, or II signals without more direct isotopic labeling methods.

The possibility of bidentate Cu^{2+} coordination by Asp1 in components Ia and Ib (Figure 5) is intriguing. CW-EPR studies of $A\beta2-16$[10] and $A\beta16$(D1N)[13] concluded that N_a coordination does occur for component I but ruled out O_c^{D1} coordination.[13] Again, this conclusion was based on an absence of any apparent changes in the principal $g_{||}$ and $A_{||}$ values in the $Cu^{2+}/A\beta16$(D1N) complex; however, it remains a possibility that another oxygen donor replaces O_c^{D1} in the mutant complex and leaves the spin Hamiltonian parameters essentially unchanged (cf. H6A, H13A, and H14A). The appearance of ^{13}C cross-peaks with $a_{iso} = -2.8$ MHz in the HYSCORE spectra of $Cu^{2+}/A\beta16(^{15}N^{13}C$-Asp1) is consistent with equatorial carboxylate oxygen coordination.[35] Moreover, destruction of a stable six-membered chelate ring formed by Asp1 in component Ia/b (Figure 5) might explain the apparent increase in the proportion of component II signal observed for $A\beta16$(D1N) compared with that of the native peptide.[13] To this end, the question of O_c^{D1} coordination in the native $Cu^{2+}/A\beta16$ complex remains unresolved. DFT modeling of the electron−nuclear hyperfine couplings between Cu^{2+} and the ^{13}C nuclei of Asp1, based on the coordination geometry of Figure 5, together with more selective ^{17}O and/or ^{13}C labeling schemes will be required to more definitively identify the oxygen ligands in $Cu^{2+}/A\beta$ complexes. We are currently synthesizing $A\beta16$ analogues with selective ^{13}C-labeling of the Asp1 carboxylate carbon, in addition to $A\beta16(^{13}C$-Asp7), $A\beta16(^{13}C$-Glu3), and $A\beta16(^{13}C$-Glu11), to systematically screen for the oxygen donors in components Ia, Ib, and II using ^{13}C HYSCORE spectroscopy.

Development of rational therapeutic strategies based upon the metallobiology of Alzheimer's disease relies on a sound understanding of the fundamental $Cu^{2+}/A\beta$ interactions at the molecular level. The pleomorphic nature of these interactions means there is the potential for small changes in local solution conditions to induce a change in the equilibria between the various coordination modes that may alter peptide structure and function. For instance, the AD brain has long been considered to be under conditions associated with acidosis,[40] which would shift the equilibrium of $Cu^{2+}/A\beta$ coordination spheres such that N-terminal coordination modes Ia and Ib are favored.

The formation of soluble oligomeric $A\beta$ species is believed to be important phenomena for modulating $A\beta$ toxicity. $A\beta$ peptides that are generated in vivo or by cultured cells occur naturally in extracellular fluids and can assemble into dimers, trimers, and higher oligomers while still at nanomolar levels.[41] There is currently no consensus from in vitro studies on how the formation or stability of these soluble oligomeric species is

(40) Heroux, M.; Raghavendra Rao, V. L.; Lavoie, J.; Richardson, J. S.; Butterworth, R. F. *Metab. Brain Dis.* **1996**, *11*, 81–88.
(41) Selkoe, D. J. *Behav. Brain Res.* **2008**, *192*, 106–113.
(42) Zou, J.; Kajita, K.; Sugimoto, N. *Angew. Chem., Int. Ed.* **2001**, *40*, 2274–2277.
(43) Barnham, K. J.; Haeffner, F.; Ciccotosto, G. D.; Curtain, C. C.; Tew, D.; Mavros, C.; Beyreuther, K.; Carrington, D.; Masters, C. L.; Cherny, R. A.; Cappai, R.; Bush, A. I. *FASEB J.* **2004**, *18*, 1427–1429.

affected by Cu^{2+} coordination,[16,42−47] and it is unclear whether the toxicity of these soluble oligomers is mediated by other cofactors in vivo.[41] However, interactions with Cu^{2+} are reported to increase the formation of protease-resistant covalently cross-linked oligomeric Aβ species,[46,43,44] increase the affinity of Aβ for lipid membranes,[48] and increase the toxicity of Aβ in neuronal cultures.[49] To date, we are unsure of the degree to which the individual coordination modes identified here contribute to these phenomena, and this work is ongoing.

Although the distribution of oligomer sizes and types was not measured, recent EPR spectroscopic studies of Aβ40 identified no major changes in $g_{||}$ and $A_{||}$ following coincubation with Cu^{2+} at pH 7.2 over a period ranging from minutes to days, strongly suggesting that Cu^{2+} coordination is independent of peptide oligomeric state.[47] The similarity of $g_{||}$ and $A_{||}$ in EPR spectra of native and mutant Cu^{2+}/Aβ complexes[9] indicates that a ligand rearrangement associated with oligomerization may not translate into significant changes in the gross $g_{||}$ and $A_{||}$ features of the EPR spectrum. Moreover, our finding that chemically distinct *native* coordination modes of monomeric Aβ can coexist with almost indistinguishable $g_{||}$ and $A_{||}$ parameters (components Ia and Ib) means that potential alterations to their distribution during or following oligomerization may also go undetected unless shf resonances can be observed. Preliminary data obtained with uniform ^{15}N-labeled Aβ40 in the presence of substoichiometric Cu^{2+} indicates that shf structure can be resolved (Figure S1 in the Supporting Information) and that aspects of the approach followed in this study could in principle be possible even in the longer aggregating peptides.

Conclusions

In this study, we demonstrated that the Cu^{2+} coordination properties of Aβ are more complicated than previously assumed. In particular, relying solely upon on the principal $g_{||}$ and $A_{||}$ parameters of components I and II is inadequate to properly characterize Cu^{2+}/Aβ complexes, even with the introduction of point mutations. We overcame this limitation by using site-specific ^{15}N-labeling to resolve the superhyperfine resonances within CW-EPR spectra and directly probe metal−ligand interactions. This revealed that the component I signal observed in CW-EPR spectra of Cu^{2+}/Aβ complexes is characterized by two interconverting 3N1O coordination modes anchored upon the amino terminus and the imidazole side chain of His6, with the third nitrogen ligand swapping between the imidazole side chains of His13 and His14. Component II signals were also found to be characterized by 3N1O coordination, where the amino terminus no longer coordinates, and the imidazole side chains of His6, His13, and His14 are ligands. Site-specific ^{17}O-labeling of Tyr10 confirmed that its phenolic oxygen does not provide an oxygen ligand in any of the coordination modes in the physiological pH range. HYSCORE spectroscopy of a Cu^{2+}/Aβ16(^{15}N^{13}C-Asp1) analogue identified ^{13}C hyperfine coupling consistent with equatorial coordination of the carboxylate oxygen of Asp1 in components Ia and Ib, but ruled out its participation in component II signals. Our findings refine a number of contradictory results in the literature regarding ligand assignments and provide valuable insight into the complexity of the metal binding properties of Aβ. Additional isotopic labeling studies of the Aβ peptide using CW- and pulsed EPR spectroscopy will enable an even more detailed picture of Cu^{2+}/Aβ interactions.

Acknowledgment. This work was supported in part by a Program Grant administered by the National Health and Medical Research Council of Australia. S.C.D. was supported by a University of Melbourne Early Career Researcher Grant. K.J.B. is a NHMRC Senior Research Fellow. Peptide synthesis was carried out by Dr. Denis Scanlon and Dr. John Karas in the Peptide Technology Facility of the Bio21 Molecular Science and Biotechnology Institute, The University of Melbourne.

Supporting Information Available: Simulations of the S-band spectra of Cu^{2+}/Aβ16(^{15}N-His13) and Cu^{2+}/Aβ16(^{15}N-His14); isolation of component II signals of Cu^{2+}/Aβ16, Cu^{2+}/Aβ16(^{15}N-His6,13,14), Cu^{2+}/Aβ16(^{15}N^{13}C-Asp1), Cu^{2+}/Aβ16(^{15}N-His6), Cu^{2+}/Aβ16(^{15}N-His13), and Cu^{2+}/Aβ16(^{15}N-His14) complexes; echo-detected EPR spectrum of Cu^{2+}/Aβ16; HYSCORE spectra of Cu^{2+}/Aβ16 and Cu^{2+}/Aβ16(^{15}N^{13}C-Asp1) at 3085 G; and CW-EPR of ^{15}N-labeled Aβ40. This material is available free of charge via the Internet at http://pubs.acs.org.

JA808073B

(44) Atwood, C. S.; Perry, G.; Zeng, H.; Kato, Y.; Jones, W. D.; Ling, K. Q.; Huang, X.; Moir, R. D.; Wang, D.; Sayre, L. M.; Smith, M. A.; Chen, S. G.; Bush, A. I. *Biochemistry* **2004**, *43*, 560–568.
(45) Garai, K.; Sengupta, P.; Sahoo, B.; Maiti, S. *Biochem. Biophys. Res. Commun.* **2006**, *345*, 210–215.
(46) Smith, D. P.; Ciccotosto, G. D.; Tew, D. J.; Fodero-Tavoletti, M. T.; Johanssen, T.; Masters, C. L.; Barnham, K. J.; Cappai, R. *Biochemistry* **2007**, *46*, 2881–2891.
(47) Karr, J. W.; Szalai, V. A. *Biochemistry* **2008**, *47*, 5006–5016.
(48) Lau, T. L.; Ambroggio, E. E.; Tew, D. J.; Cappai, R.; Masters, C. L.; Fidelio, G. D.; Barnham, K. J.; Separovic, F. *J. Mol. Biol.* **2006**, *356*, 759–770.
(49) Cuajungco, M. P.; Goldstein, L. E.; Nunomura, A.; Smith, M. A.; Lim, J. T.; Atwood, C. S.; Huang, X.; Farrag, Y. W.; Perry, G.; Bush, A. I. *J. Biol. Chem.* **2000**, *275*, 19439–19442.